

Mechanism of Delocalization-Enhanced Exciton Transport in Disordered Organic Semiconductors

Daniel Balzer and Ivan Kassal*



Cite This: *J. Phys. Chem. Lett.* 2023, 14, 2155–2162



Read Online

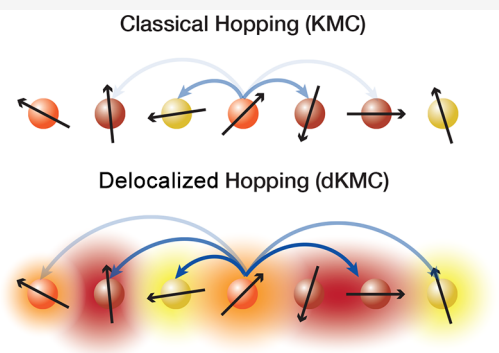
ACCESS |

Metrics & More

Article Recommendations

Supporting Information

ABSTRACT: Large exciton diffusion lengths generally improve the performance of organic semiconductor devices, because they enable energy to be transported farther during the exciton lifetime. However, the physics of exciton motion in disordered organic materials is not fully understood, and modeling the transport of quantum-mechanically delocalized excitons in disordered organic semiconductors is a computational challenge. Here, we describe delocalized kinetic Monte Carlo (dKMC), the first model of three-dimensional exciton transport in organic semiconductors that includes delocalization, disorder, and polaron formation. We find that delocalization can dramatically increase exciton transport; for example, delocalization across less than two molecules in each direction can increase the exciton diffusion coefficient by over an order of magnitude. The mechanism for the enhancement is 2-fold: delocalization enables excitons to hop both more frequently and further in each hop. We also quantify the effect of transient delocalization (short-lived periods where excitons become highly delocalized) and show that it depends strongly upon the disorder and transition dipole moments.



Efficient energy transport, in the form of excitons, is essential to the performance of organic semiconductor devices, including solar cells, light-emitting diodes, and flexible electronics.^{1–6} However, continued development of materials with large exciton diffusion lengths is limited by theoretical and computational models of exciton transport that lack important features. In particular, excitons are often assumed to be localized onto individual molecules and to hop between them via Förster resonant energy transfer (FRET).^{4,7–11} However, the assumption of localized excitons often fails, leading to underestimates of how far excitons can travel.¹¹ Instead, the movement of excitons often falls into the theoretically awkward intermediate regime between completely localized excitons (described using FRET) and completely delocalized excitons (described using band transport).

Recent studies have significantly improved the modeling of partially delocalized excitons in the intermediate regime, showing that delocalization improves exciton transport. These studies have ranged from detailed atomistic approaches using multi-configurational time-dependent Hartree (MCTDH)^{12–15} to approaches that balance accuracy and performance to extend the simulations to larger length or time scales, including quantum master equations^{16–21} and surface hopping.^{22–25} It has been proposed that delocalization enhancements of exciton transport are caused by short periods of large delocalization, dubbed transient delocalization.^{22,23,26} In particular, Sneyd et al. hypothesized that large diffusion coefficients in one-dimensional (1D) poly(3-hexylthiophene) (P3HT) nanofiber films were a consequence of transient

delocalization, after observing individual calculated exciton trajectories in which otherwise localized excitons occasionally moved a large distance through brief transitions to highly delocalized states.²³ In the context of exciton transport in organic crystals, Giannini et al. showed that ignoring delocalization events reduced the diffusion coefficient 3-fold.²²

However, the basic mechanism of delocalization-enhanced exciton transport remains incompletely understood, largely because computational complexity of existing techniques limits simulations to individual materials, low dimensions, short times, short length scales, or few trajectories. Conclusively establishing that diffusion enhancements are caused by delocalization requires a method that can go beyond studying individual materials and can predict trends across wide parameter ranges while reproducing localized hopping in the correct limits. Similarly, determining whether delocalization enhancements are caused by large enhancements to a few events (as suggested by the hypothesis of transient delocalization) or smaller enhancements to many events requires a way to quantify transient delocalization. To understand the role of delocalization in organic devices

Received: December 22, 2022

Accepted: February 16, 2023

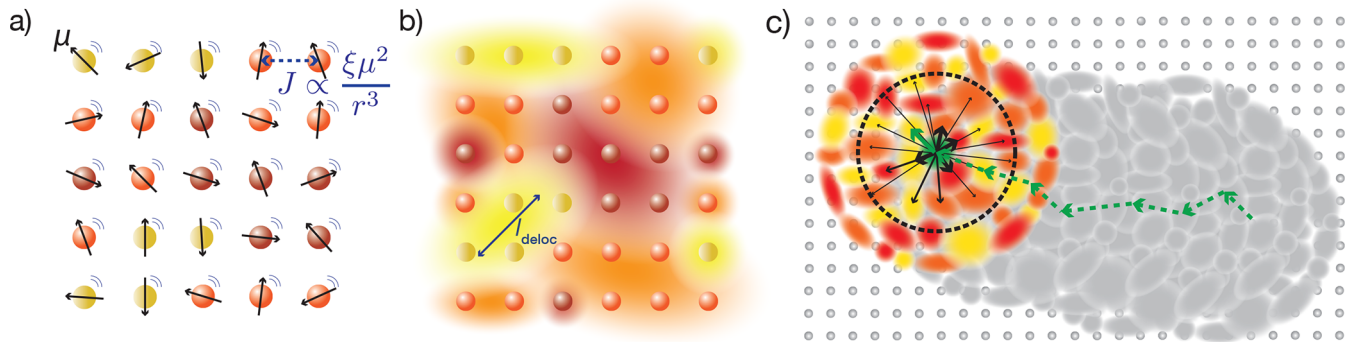


Figure 1. dKMC model of exciton transport. (a) Exciton transport is modeled on a regular lattice of sites (spheres) with randomly oriented transition dipole moments μ and disordered energies (different colors). Sites are coupled to each other with dipole–dipole coupling J and to an environment (motion lines). (b) Diagonalizing the polaron-transformed Hamiltonian produces the partially delocalized excitonic states (clouds; only some states shown), whose size depends upon the strength of the disorder, the excitonic couplings, and the coupling to the environment. (c) dKMC propagates the dynamics through the excitonic states by tracking and averaging over individual trajectories (green line) through large systems. At each step, polaron states are only calculated within a small neighborhood, and the destination state is chosen probabilistically from the outgoing rates (arrows), which are only calculated for states within a cutoff distance (black dotted line).

requires the ability to model delocalized exciton motion in mesoscopic three-dimensional systems over realistic transport time scales.

Here, we solve these problems by developing delocalized kinetic Monte Carlo (dKMC), the first model of three-dimensional exciton transport that includes the essential ingredients of disorder, delocalization, and polaron formation. Our algorithm is based on our dKMC for charge transport;^{27,28} although the equations of motion are similar, exciton dynamics is significantly different from that of charges because of the long-range nature of excitonic couplings. The numerical performance of dKMC allows us to scan wide parameter ranges to establish that delocalization improves exciton motion on long time and length scales and in the three dimensions inaccessible to some previous techniques. We show that the delocalization enhancement is a consequence of both increased hopping distances and frequencies and not just one factor alone. Lastly, we develop a general method to quantify the contributions of transient delocalization events, showing that the impact of transient delocalization depends strongly upon the energetic disorder and the molecular transition dipole moments.

We model the transport of excitons on a regular, d -dimensional lattice of N^d sites (Figure 1a). The energies E_n of the sites are disordered, chosen randomly from a Gaussian distribution, $g(E) = \exp(-(E - E_0)^2/2\sigma^2)/\sqrt{2\pi\sigma^2}$, whose standard deviation σ is the excitonic disorder.²⁹ Each site is also assigned a transition dipole moment μ_n with constant magnitude μ but random orientation. The sites are coupled to each other by the dipole–dipole interaction, $J_{mn} = \xi_{mn}\mu_m^2/4\pi\varepsilon_0|\mathbf{R}_{mn}|^3$, where \mathbf{R}_{mn} is the distance vector between sites m and n and ξ_{mn} is the orientation factor, $\xi_{mn} = \hat{\mu}_m \cdot \hat{\mu}_n - 3(\hat{\mathbf{R}}_{mn} \cdot \hat{\mu}_m)(\hat{\mathbf{R}}_{mn} \cdot \hat{\mu}_n)$, where hats indicate corresponding unit vectors. The random orientation of the dipole moments produces (off-diagonal) disorder in the excitonic couplings, because they depend strongly upon the orientation of the two dipoles. The Hamiltonian describing the system is then given by

$$H_S = \sum_n E_n |n\rangle\langle n| + \sum_{m \neq n} J_{mn} |m\rangle\langle m| \quad (1)$$

The environment is treated as an independent bath of harmonic oscillators on every site^{4,8}

$$H_B = \sum_{n,k} \omega_{nk} b_{nk}^\dagger b_{nk} \quad (2)$$

where ω_{nk} is the frequency of mode k on site n , with creation and annihilation operators b_{nk}^\dagger and b_{nk} . The system–bath interaction is described with a linear coupling of each site to its bath modes

$$H_{SB} = \sum_{n,k} g_{nk} |n\rangle\langle n| (b_{nk}^\dagger + b_{nk}) \quad (3)$$

We account for the formation of (excitonic) polarons, quasi-particles containing the exciton, and the associated distortion to the bath.^{30,31} Polaron formation is included in the model by applying the polaron transformation³²

$$e^S = \exp \left(\sum_{n,k} \frac{g_{nk}}{\omega_{nk}} |n\rangle\langle n| (b_{nk}^\dagger - b_{nk}) \right) \quad (4)$$

to the entire Hamiltonian, giving $\tilde{H}_{tot} = e^S H_{tot} e^{-S} = \tilde{H}_S + \tilde{H}_B + \tilde{H}_{SB}$. The transformation displaces the bath modes, giving the transformed system Hamiltonian

$$\tilde{H}_S = \sum_n \tilde{E}_n |n\rangle\langle n| + \sum_{m \neq n} J_{mn} \kappa_{mn} |m\rangle\langle m| \quad (5)$$

where $\tilde{E}_n = E_n - \sum_k \lg_{nk}^2 / \omega_k$ and the excitonic couplings are renormalized by

$$\kappa_{mn} = e^{-\frac{1}{2} \sum_k \left(\frac{g_{mk}}{\omega_{mk}}^2 \coth \left(\frac{\omega_{mk}}{2k_B T} \right) + \frac{g_{nk}}{\omega_{nk}}^2 \coth \left(\frac{\omega_{nk}}{2k_B T} \right) \right)} \quad (6)$$

where T is the temperature. The bath Hamiltonian is unaffected, $\tilde{H}_B = H_B$, and the system–bath Hamiltonian becomes $\tilde{H}_{SB} = \sum_{n \neq m} J_{mn} |m\rangle\langle n| V_{mn}$, where $V_{mn} = \exp \left(\sum_k \frac{g_{mk}}{\omega_{mk}} (b_{mk}^\dagger - b_{mk}) - \sum_k \frac{g_{nk}}{\omega_{nk}} (b_{nk}^\dagger - b_{nk}) \right) - \kappa_{mn}$.

For simplicity, we assume the same system–bath interaction on all sites, $g_{nk} = g_k$ with spectral density $J(\omega) =$

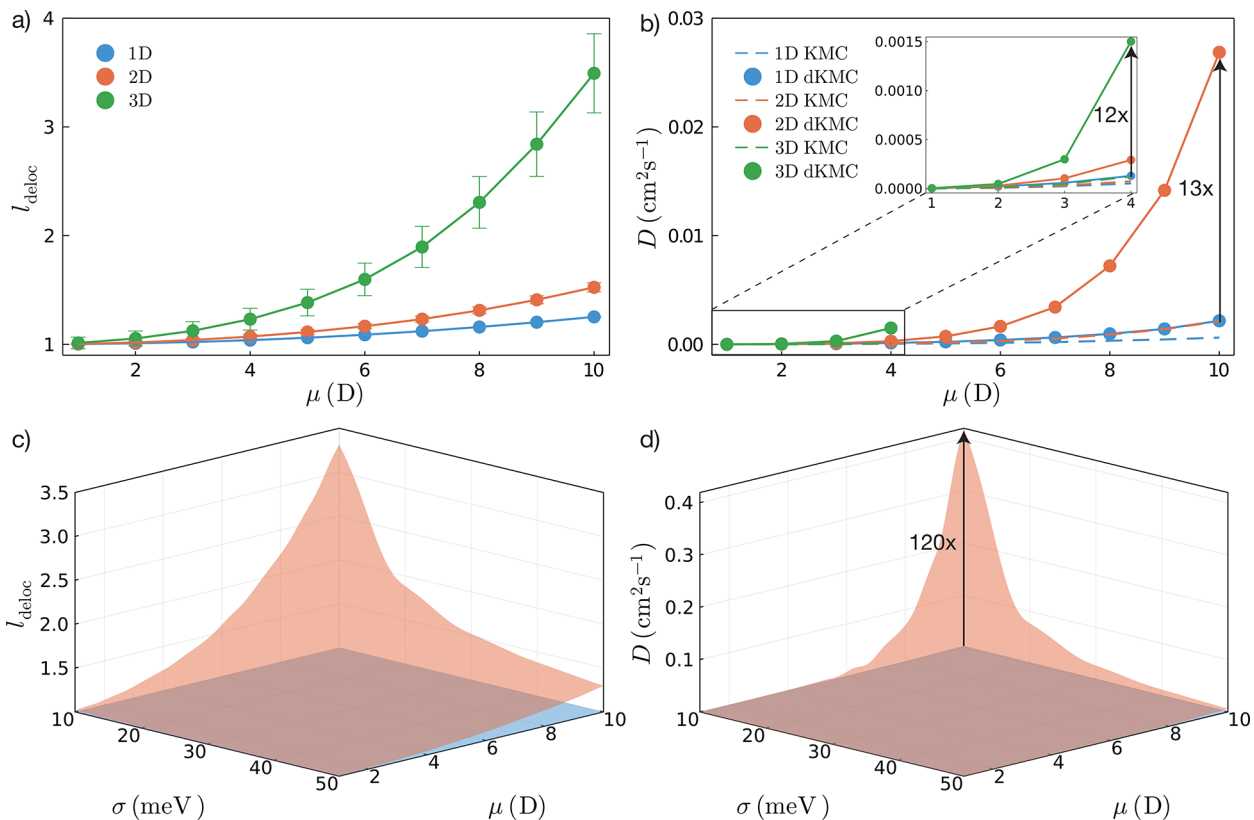


Figure 2. Delocalization enhances exciton transport. (a) Delocalization length l_{deloc} of excitonic states increases with the transition dipole moment μ in all dimensions (shown for $\sigma = 30 \text{ meV}$). (b) Exciton diffusion coefficient D as a function of μ , predicted without (KMC) and with (dKMC) delocalization, for $\sigma = 30 \text{ meV}$. In all dimensions, the dKMC diffusion coefficient is larger and increases faster with μ compared to that predicted by KMC. This delocalization enhancement is greater in higher dimensions. The error bars are the standard errors of the mean. (c) Delocalization length l_{deloc} and (d) diffusion coefficient D predicted by KMC (blue) and dKMC (orange), for varying σ and μ in two dimensions. Both the extent of delocalization (l_{deloc}) and the delocalization enhancement of D increase with both increasing μ and decreasing σ .

$\sum_k g_k^{-2} \delta(\omega - \omega_k)$.⁸ Doing so simplifies the renormalization factor to

$$\kappa_{mn} = \kappa = \exp\left(-\int_0^\infty d\omega \frac{J(\omega)}{\omega^2} \coth(\omega/2k_B T)\right) \quad (7)$$

We use a super-ohmic spectral density $J(\omega) = \frac{\lambda}{2}(\omega/\omega_c)^3 \exp(-\omega/\omega_c)$,^{33–36} with a reorganization energy of $\lambda = 150 \text{ meV}$ of each molecule (which is within the range of typical values found in organic semiconductors^{11,21,22,25}) and a cutoff frequency $\omega_c = 62 \text{ meV}$.³⁷

After the polaron transformation, we diagonalize \tilde{H}_S to find its eigenstates, namely, the polaron states ν (Figure 1b). Because $\kappa < 1$, the polaron transformation reduces the excitonic couplings, meaning that polaronic states are smaller than those of the bare excitons,³⁸ simplifying the calculation. The polaron transformation also absorbs most of the system–bath interaction into the polaron itself, after which the reduced system–bath coupling is treated as a perturbation to second order.^{32–34,39–47} As detailed previously,^{27,46} the result of the perturbative treatment is the secular polaron-transformed Redfield equation (sPTRE)⁴⁶

$$\frac{d\rho_{\nu\nu}(t)}{dt} = \sum_{\nu'} R_{\nu\nu'} \rho_{\nu'\nu}(t) \quad (8)$$

a master equation for the polaron-state populations $\rho_{\nu\nu}(t)$. The Redfield transition rates

$$R_{\nu\nu'} = 2\text{Re} \Gamma_{\nu'\nu,\nu\nu'} - \delta_{\nu\nu'} \sum_{\kappa} 2\text{Re} \Gamma_{\nu\kappa,\kappa\nu} \quad (9)$$

describe the bath-induced relaxation in terms of the damping rates

$$\begin{aligned} \Gamma_{\mu\nu,\mu'\nu'} &= \sum_{m,n,m',n'} J_{mn} J_{m'n'} \\ &\langle \mu|lm\rangle \langle nl\nu' \rangle \langle \mu'|lm' \rangle \langle n'l\nu' \rangle K_{mn,m'n'}(\omega_{\nu'\mu'}) \end{aligned} \quad (10)$$

where $K_{mn,m'n'}(\omega) = \int_0^\infty e^{i\omega\tau} \langle \tilde{V}_{mn}(\tau) \tilde{V}_{m'n'}(0) \rangle_B d\tau$ is the half-Fourier transform of the bath correlation function $\langle \tilde{V}_{mn}(\tau) \tilde{V}_{m'n'}(0) \rangle_B = \kappa^2 (e^{\lambda_{mn,m'n'}\varphi(\tau)} - 1)$, where $\lambda_{mn,m'n'} = \delta_{m'm} - \delta_{mn'} + \delta_{n'n} - \delta_{nm}$ and $\varphi(\tau) = \int_0^\infty d\omega \frac{J(\omega)}{\omega^2} (\cos(\omega\tau) \coth(\beta\omega/2) - i \sin(\omega\tau))$.³⁴

Solving eq 8 to calculate the dynamics of all of the excitons is only computationally tractable for small systems. Instead, we use dKMC,^{27,28} which stochastically unravels the master equation onto kinetic Monte Carlo and improves the numerical performance using distance-based cutoffs enabled by the limited polaron sizes. Here, we summarize the algorithm, given in full in section S1 of the Supporting Information. First, we select a random disordered landscape of N^d sites from the distributions described above, and then and

throughout the simulation we diagonalize subsets of this landscape to only find polaron states close to the current location of the exciton (Figure 1c). Then, Redfield rates $R_{\nu\nu'}$ for hopping from the current state ν are only calculated for destination states ν' that lie within a certain cutoff radius. In calculating each of these rates, we truncate the sum in eq 10 to only include sites contributing the most to the populations of each state, i.e., the fewest sites m such that $\sum_m |\langle \mu | m \rangle|^2$ exceeds a population cutoff. Both of these cutoffs are adjusted to obtain a target accuracy. The destination state is chosen probabilistically among the possible targets, in proportion to the corresponding hopping rates, as in a standard kinetic Monte Carlo. The procedure is repeated until a chosen final time t_{end} , giving an individual exciton trajectory. The simulation is then repeated for many trajectories on many realizations of disorder to obtain sufficient statistics and allow the exciton diffusion coefficient to be calculated as

$$D = \frac{d}{dt} \left(\overline{\langle r^2(t) \rangle} \right) \Big|_{t=t_{\text{end}}} \quad (11)$$

where $\overline{\langle r^2(t) \rangle}$ is the mean-squared exciton displacement, averaged over trajectories (angle brackets) and realizations of disorder (overline).

In disordered materials, such as those considered here, D is, strictly speaking, a time-dependent quantity. Transport in disordered materials is dispersive: as the exciton is given more time to explore a disordered landscape, its energy will steadily decrease as it finds deeper energetic traps, which it must escape, reducing the diffusion coefficient as time continues. Therefore, it is necessary to specify an end time t_{end} at which D is calculated. In this work, we use $t_{\text{end}} = 100$ ps, a typical excitonic transit time for typical length scales in organic semiconductors.

All approximations in dKMC are conservative; i.e., they underestimate the extent and effect of delocalization, as detailed in section S2 of the Supporting Information. In particular, distance-based cutoffs required by dKMC lead to an underestimation of delocalization effects, as does the finite simulation time scale t_{end} . Although some excitons move on longer time scales, increasing t_{end} would also increase delocalization enhancements.

To determine the effect of delocalization on exciton transport, we vary two key parameters: the transition dipole moment μ and the excitonic disorder σ . All other simulation parameters are outlined in section S3 of the Supporting Information. Figure 2a shows that increasing μ increases the exciton delocalization, especially in higher dimensions. We quantify the delocalization using the delocalization length

$$l_{\text{deloc}} = \overline{\text{IPR}}_{\nu}^{-1/d} \quad (12)$$

where $\overline{\text{IPR}}_{\nu}$ is the average inverse participation ratio of the polaron states.

$$\text{IPR}_{\nu} = \left(\sum_n |\langle n | \nu \rangle|^4 \right)^{-1} \quad (13)$$

The IPR roughly corresponds to the number of sites an excitonic state extends over. Therefore, l_{deloc} measures to the extent of an excitonic state in each direction, enabling comparisons between different dimensions. The considerably

larger l_{deloc} in three dimensions indicates the importance of fully three-dimensional (3D) simulations.

Delocalization significantly increases exciton diffusion, especially in higher dimensions (Figure 2b). In each dimension, the diffusion coefficients predicted by KMC and dKMC agree at low μ , where the electronic states are localized. As μ increases, D_{dKMC} becomes larger than D_{KMC} , demonstrating that delocalization enhances exciton transport. For $\mu = 10$ D in two dimensions, delocalization across less than two molecules in each direction ($l_{\text{deloc}} = 1.5$) gives a delocalization enhancement of $D_{\text{dKMC}}/D_{\text{KMC}} = 13$. Furthermore, the delocalization enhancement is greater in higher dimensions if all parameters are held fixed. In three dimensions, despite the large computational savings, dKMC is limited to small μ because the excitonic states become too large to be contained within computationally tractable boxes.

Our conclusions about the importance of delocalization are general, holding at all typical values of excitonic disorder. In particular, at any σ , increasing μ increases the IPR, the diffusion coefficient D , and the enhancement $D_{\text{dKMC}}/D_{\text{KMC}}$ (shown for two dimensions in panels c and d of Figure 2). These parameter scans also show the deleterious effect of disorder on exciton diffusion; increasing σ reduces both IPR and D at constant μ .

The mechanism of delocalization-enhanced exciton transport is 2-fold: excitons both hop further in each hop, and they hop more frequently, two contributions that are distinguished in Figure 3. The first mechanism is that delocalized excitons hop further in each hop, on average, than localized excitons. Figure 3a shows that the mean-squared hopping distance $\langle d_{\text{hop}}^2 \rangle$ grows as a function of μ in both KMC and dKMC but much more rapidly for the latter. The parameter scan in Figure 3c repeats the same calculation at various values of σ , showing that $\langle d_{\text{hop}}^2 \rangle$ increases with both increasing μ and decreasing σ . As μ increases or σ decreases (or both), the excitons become more delocalized, increasing their coupling to exciton states that are further away, thus enabling them to hop further in one hop. Furthermore, the longer distance couplings provide more possible hopping destinations, increasing the likelihood of finding an energetically favorable (and thus faster) transition. The second mechanism of delocalization-enhanced transport is that the rate of hopping between delocalized excitons is greater on average, reducing the time between transitions. Figure 3b shows the average sum of transition rates for hops leaving a particular state, $\langle \sum_{\nu'} R_{\nu\nu'} \rangle$, as a function of μ . As μ increases, $\langle \sum_{\nu'} R_{\nu\nu'} \rangle$ increases in both KMC and dKMC but considerably faster in dKMC. The calculation is repeated in Figure 3d for $\langle \sum_{\nu'} R_{\nu\nu'} \rangle$ but as a function of both μ and σ .

Both mechanisms are necessary to explain the large delocalization enhancements seen in panels b and d of Figure 2. For example, for the parameter values in panels a and b of Figure 3, the enhancement to $\langle d_{\text{hop}}^2 \rangle$ is 3×, while that to $\langle \sum_{\nu'} R_{\nu\nu'} \rangle$ is 4×, neither of which is sufficient to explain the 12× or 13× enhancement to D in Figure 2b. However, by dimensional analysis, the enhancement to D should be proportional to the product of the enhancements to $\langle d_{\text{hop}}^2 \rangle$ and $\langle \sum_{\nu'} R_{\nu\nu'} \rangle$. Indeed, the product of the 3× and 4× enhancements accounts for the overall 12–13× enhancement in D . Similarly, over the greater parameter range in panels c and d of Figure 3, multiplying the 25× enhancement to $\langle d_{\text{hop}}^2 \rangle$ with the 4.5× enhancement to $\langle \sum_{\nu'} R_{\nu\nu'} \rangle$ explains the overall 120× enhancement to D seen in Figure 2d.

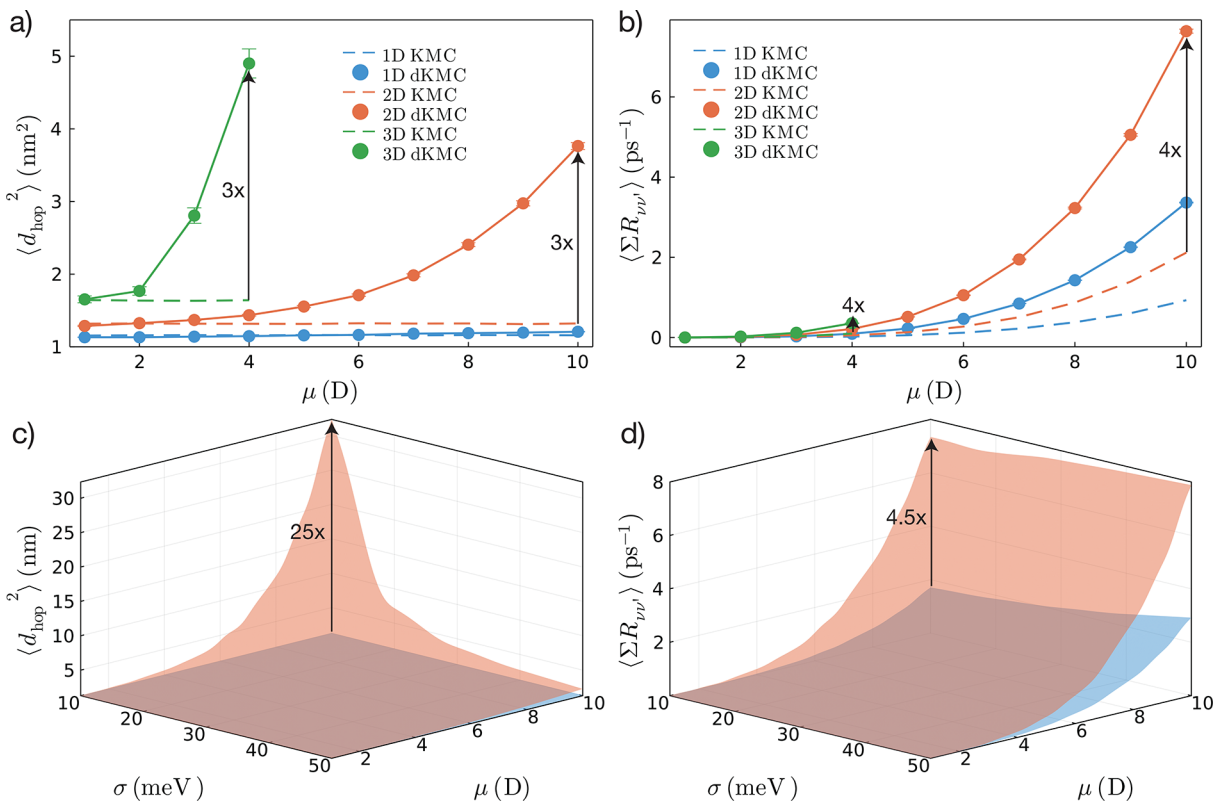


Figure 3. Mechanism of delocalization-enhanced exciton transport. (a) Mean-squared hopping distance $\langle d_{\text{hop}}^2 \rangle$ and (b) mean outgoing rate sum $\langle \sum R_{\nu\nu'} \rangle$ as functions of the transition dipole moment μ for dKMC and KMC in each dimension. As delocalization increases with increasing μ , the dKMC values of both $\langle d_{\text{hop}}^2 \rangle$ and $\langle \sum R_{\nu\nu'} \rangle$ grow faster than their KMC (localized-hopping) versions. When the enhancements to $\langle d_{\text{hop}}^2 \rangle$ and $\langle \sum R_{\nu\nu'} \rangle$ are multiplied, they account for the total delocalization enhancement to D seen in Figure 2b. Similarly, (c) $\langle d_{\text{hop}}^2 \rangle$ and (d) $\langle \sum R_{\nu\nu'} \rangle$ as functions of both μ and the disorder σ for dKMC (orange) and KMC (blue) in two dimensions. As in panels a and b, multiplying the enhancements to $\langle d_{\text{hop}}^2 \rangle$ and $\langle \sum R_{\nu\nu'} \rangle$ accounts for the delocalization enhancement to D in Figure 2d.

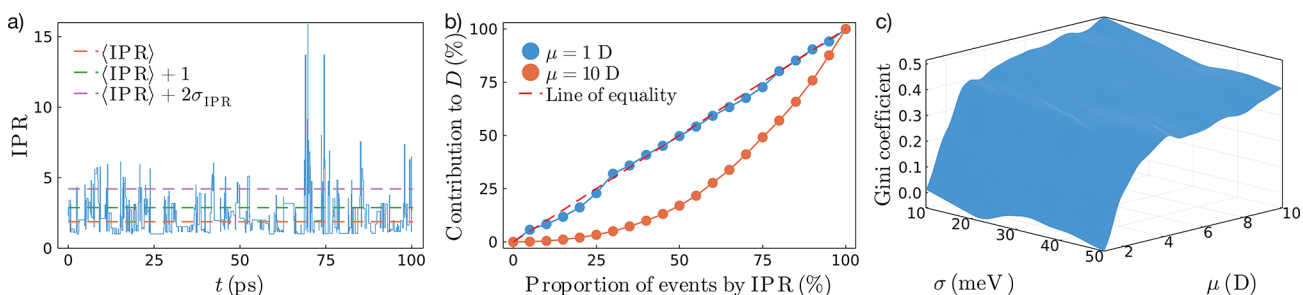


Figure 4. Quantifying transient delocalization. (a) IPR of an exciton over a single trajectory in 2D with $\mu = 10$ D. Most of the time, the IPR of an exciton is near the average $\langle \text{IPR} \rangle$, but occasionally, it briefly delocalizes a large amount, known as transient delocalization. (b) Lorenz curves showing the cumulative contributions to D of the bottom $x\%$ of hopping events, ranked by IPR. The line of equality represents exciton transport where every hopping event contributes equally to D . The Gini coefficient quantifies how disproportionate the contributions from highly delocalized events are; it is twice the area between the Lorenz curve and the line of equality. In the more localized example ($\mu = 1$ D), a low Gini coefficient $G = 0.01$ implies insignificant transient delocalization. In the more delocalized example ($\mu = 10$ D), the higher value $G = 0.43$ demonstrates a greater importance for transient delocalization events; for instance, 25% of the most delocalized hopping events account for 51% of D . (c) Gini coefficients for a range of μ and σ in 2D, showing that the importance of transient delocalization depends strongly upon the parameters.

Although the average enhancements can be explained using the mechanisms above, averages do not tell the whole story, and to understand transport, we also need to look at distributions. The delocalization of an exciton is not fixed but can fluctuate rapidly and by a large amount from the mean $\langle \text{IPR} \rangle$ (Figure 4a). Transient delocalization is the hypothesis that these fluctuations are important, i.e., that a few hops involving highly delocalized states contribute disproportionately to the delocalization enhancement to D , whereas the

alternative would be that the delocalization enhancement was caused by smaller improvements to many (or all) of the hops.

Distinguishing these two possibilities requires a way to measure the inequality of distributions. To do so, we use the Lorenz curve, a plot of the cumulative distribution function commonly used in economics to quantify the inequality of wealth distributions.^{48,49} In studying wealth distributions, the Lorenz curve shows the fraction of the wealth owned by the bottom $x\%$ of the population, i.e., the cumulative proportion of the total wealth held by a cumulative proportion of the total

population (ranked by wealth). If every person had an equal amount of wealth, the Lorenz curve would be a straight line known as the line of equality. Departures from equal distributions are measured by the Gini coefficient G , which is twice the area between the line of equality and the Lorenz curve. A fully equal wealth distribution has a Gini coefficient of 0, and the wealth inequality grows as the Gini coefficient increases, up to its maximum value of 1.

To quantify the inequality of distributions of exciton hops based on the extent of delocalization, we plot the cumulative contribution to the diffusion constant D of the cumulative proportion of hopping events, ranked by IPR (Figure 4b). To construct this Lorenz curve, we assign to each hop the greater of the IPRs of the donor and acceptor states, and then we rank all of the hops in all of the trajectories based on this IPR. To calculate the contribution of the bottom $x\%$ of hops, we construct new trajectories where the top $(100 - x)\%$ of hops are removed; i.e., we connect together the displacement vectors of the retained hops. The diffusion coefficient predicted by these new trajectories is the contribution to the total D that can be assigned to the bottom $x\%$ hops. Unlike Lorenz curves for wealth inequality, our Lorenz curve may, in exceptional cases, rise above the line of equality because it is possible (although rare) for states with smaller IPR to contribute more to D than larger states. Nevertheless, the Gini coefficient remains a useful measure of the disproportionate influence of transient delocalization effects.

Panels b and c of Figure 4 show that the Gini coefficient is smaller for relatively localized systems and larger for delocalized systems, whether the delocalization is caused by large μ or small σ (or both). Therefore, the importance of transient delocalization depends strongly upon the parameter regime: in disordered systems with weak couplings, it can be negligible, and it only becomes significant in organic semiconductors that are relatively ordered and have strong couplings among sites. This agrees with the finding that transient delocalization can have a large effect in organic crystals,²² where disorder is low and couplings are large.

Quantifying transient delocalization with the Gini coefficient has the advantage of taking into account the entire distribution of trajectories. In contrast, initial approaches to transient delocalization²³ only identified individual transient delocalization events in particular trajectories, which cannot be guaranteed to be typical, especially in disordered materials where individual trajectories can behave very differently. More recent work classified events as transient delocalization or not;²² however, doing so requires an arbitrary cutoff and discards information contained in the full distribution. For example, IPR fluctuations to $\langle \text{IPR} \rangle + 1$ may be sufficiently rare to classify such events as transient delocalization in one material²² but insufficient in another material with larger fluctuations. For example, Figure 4a shows a material where a cutoff of $\text{IPR} = \langle \text{IPR} \rangle + 1$ would label as many as 24% of events as transient delocalization, meaning that they are no longer remarkable, rare events. A more generic definition might have a cutoff that depends upon the spread of the IPRs, setting the limit of transient delocalization at $\text{IPR} = \langle \text{IPR} \rangle + w\sigma_{\text{IPR}}$, where $w = 1$ has been used when studying charge transport to characterize the time between wave function delocalization events,⁵⁰ but even this requires an arbitrary choice of how many standard deviations w should be considered. Because our method applies to any distribution

of events, it can quantify transient delocalization in all parameter regimes (Figure 4).

Overall, the computational performance of dKMC has enabled some of the largest simulations of delocalized exciton transport in disordered materials. Previously, the largest such simulations were two-dimensional (2D) simulations of about 300 molecules for 1 ps;²² in contrast, we simulated 3D systems with millions of sites for 100 ps. In addition, the speed of dKMC allows predictions of general trends over large parameter ranges, which have yielded the mechanistic insights above.

This gain in computational performance requires a series of approximations that can be limiting in some cases. Many of the assumptions in dKMC come from the underlying master equation, sPTRE. While sPTRE is accurate in the parameter ranges studied here, it loses accuracy when the system is weakly coupled to a slow bath, where the exciton dynamics occurs faster than the bath relaxation, preventing the relaxed-bath assumption of the fully displaced polaron transformation.^{33,37,46,51} As an alternative, the variational polaron transformation^{33,52–54} would allow dKMC to be more accurately applied to a system weakly coupled to slow baths or to an ohmic or sub-ohmic bath. Similarly, sPTRE uses the secular approximation to neglect coherences between states and justify tracking only the polaron populations. The approximation is justified because coherences are unlikely to be induced in incoherent light,^{55–62} and even if they were, they would be unlikely to survive on exciton-transport time scales. However, if required, dKMC could be adapted to include coherences. A final assumption is the local (diagonal) system–bath coupling, which is usually made in disordered organic semiconductors.^{4,8} However, in organic crystals, non-local (off-diagonal) system–bath couplings become important as they introduce dynamic disorder in the electronic couplings, which can be relevant on the fast transport time scales in organic crystals.¹⁷ Relaxing the local-bath assumption would require a significant adjustment to the sPTRE equations of motions, because the polaron transformation relies on the ability to remove diagonal system–bath couplings.

dKMC could be applied to explain the exciton-transport behavior of specific disordered materials using multiscale simulation. dKMC input parameters, σ , μ , λ , and ω_c , can be calculated for specific materials using atomistic quantum-chemistry simulations, as has been done for other effective Hamiltonian models of exciton transport.^{20,22,24,25}

We anticipate that dKMC will also be applied to describe related processes in optoelectronic materials, including exciton recombination, exciton dissociation, and singlet fission. Eventually, we expect that it will be possible to incorporate delocalization into mesoscopic simulation of all optoelectronic processes relevant to organic electronics and, through rates predicted by dKMC or simplifications, such as jKMC,⁶³ into device-scale drift-diffusion models.

In conclusion, dKMC describes mesoscale 3D exciton transport in organic semiconductors, for the first time, including the important ingredients of disorder, delocalization, and polaron formation. Our simulations show that delocalization significantly improves exciton transport over classical hopping, especially in higher dimensions. We showed that this enhancement is a combined effect of larger average hopping distances and outgoing rates, and we quantified the contribution of transient delocalization, finding that its importance depends strongly upon the nature of the material.

We anticipate that these mechanistic insights will aid in the discovery of improved exciton-transport materials and that our simulation techniques can be further extended to address other open questions in organic optoelectronics.

■ ASSOCIATED CONTENT

SI Supporting Information

The Supporting Information is available free of charge at <https://pubs.acs.org/doi/10.1021/acs.jpcllett.2c03886>.

Details of dKMC (section S1), choices of accuracy and end time (section S2), and simulation parameters (section S3) ([PDF](#))

■ AUTHOR INFORMATION

Corresponding Author

Ivan Kassal – School of Chemistry, University of Sydney, Sydney, New South Wales 2006, Australia;  orcid.org/0000-0002-8376-0819; Email: ivan.kassal@sydney.edu.au

Author

Daniel Balzer – School of Chemistry, University of Sydney, Sydney, New South Wales 2006, Australia

Complete contact information is available at: <https://pubs.acs.org/10.1021/acs.jpcllett.2c03886>

Notes

The authors declare no competing financial interest.

■ ACKNOWLEDGMENTS

The authors were supported by a Westpac Scholars Trust Future Leaders Scholarship, the Australian Research Council (DP220103584), the Australian Government Research Training Program, and computational resources from the National Computational Infrastructure (Gadi) and the University of Sydney Informatics Hub (Artemis).

■ REFERENCES

- (1) Brédas, J.-L.; Beljonne, D.; Coropceanu, V.; Cornil, J. Charge-transfer and energy-transfer processes in π -conjugated oligomers and polymers: A molecular picture. *Chem. Rev.* **2004**, *104*, 4971–5004.
- (2) Menke, S. M.; Holmes, R. J. Exciton diffusion in organic photovoltaic cells. *Energy Environ. Sci.* **2014**, *7*, 499–512.
- (3) Mikhnenko, O. V.; Blom, P. W. M.; Nguyen, T.-Q. Exciton diffusion in organic semiconductors. *Energy Environ. Sci.* **2015**, *8*, 1867–1888.
- (4) Köhler, A.; Bässler, H. *Electronic Processes in Organic Semiconductors: An Introduction*; Wiley-VCH Verlag GmbH & Co. KGaA: Weinheim, Germany, 2015; DOI: [10.1002/9783527685172](https://doi.org/10.1002/9783527685172).
- (5) Bjørgaard, J. A.; Köse, M. E. Simulations of singlet exciton diffusion in organic semiconductors: A review. *RSC Adv.* **2015**, *5*, 8432–8445.
- (6) Dimitriev, O. P. Dynamics of excitons in conjugated molecules and organic semiconductor systems. *Chem. Rev.* **2022**, *122*, 8487–8593.
- (7) Förster, T. Intermolecular energy migration and fluorescence. *Ann. Phys.* **1948**, *437*, 55–75.
- (8) May, V.; Kühn, O. *Charge and Energy Transfer Dynamics in Molecular Systems*, 3rd ed.; Wiley-VCH Verlag GmbH & Co. KGaA: Weinheim, Germany, 2011; DOI: [10.1002/9783527633791](https://doi.org/10.1002/9783527633791).
- (9) Athanasopoulos, S.; Emelianova, E. V.; Walker, A. B.; Beljonne, D. Exciton diffusion in energetically disordered organic materials. *Phys. Rev. B* **2009**, *80*, 195209.
- (10) Stehr, V.; Fink, R. F.; Engels, B.; Pflaum, J.; Deibel, C. Singlet exciton diffusion in organic crystals based on marcus transfer rates. *J. Chem. Theory Comput.* **2014**, *10*, 1242–1255.
- (11) Hume, P. A.; Jiao, W.; Hodgkiss, J. M. Long-range exciton diffusion in a non-fullerene acceptor: Approaching the incoherent limit. *J. Mater. Chem. C* **2021**, *9*, 1419–1428.
- (12) Binder, R.; Wahl, J.; Römer, S.; Burghardt, I. Coherent exciton transport driven by torsional dynamics: A quantum dynamical study of phenylene-vinylene type conjugated systems. *Faraday Discuss.* **2013**, *163*, 205–222.
- (13) Wahl, J.; Binder, R.; Burghardt, I. Quantum dynamics of ultrafast exciton relaxation on a minimal lattice. *Comput. Theor. Chem.* **2014**, *1040–1041*, 167–176.
- (14) Binder, R.; Burghardt, I. First-principles description of intra-chain exciton migration in an oligo(*para*-phenylene vinylene) chain. *J. Chem. Phys.* **2020**, *152*, 204120.
- (15) Popp, W.; Brey, D.; Binder, R.; Burghardt, I. Quantum dynamics of exciton transport and dissociation in multichromophoric systems. *Annu. Rev. Phys. Chem.* **2021**, *72*, 591–616.
- (16) Janković, V.; Vukmirović, N. Dynamics of exciton formation and relaxation in photoexcited semiconductors. *Phys. Rev. B* **2015**, *92*, 235208.
- (17) Aragó, J.; Troisi, A. Regimes of exciton transport in molecular crystals in the presence of dynamic disorder. *Adv. Funct. Mater.* **2016**, *26*, 2316–2325.
- (18) Shi, L.; Willard, A. P. Modeling the effects of molecular disorder on the properties of Frenkel excitons in organic molecular semiconductors. *J. Chem. Phys.* **2018**, *149*, 094110.
- (19) Lee, C. K.; Shi, L.; Willard, A. P. Modeling the influence of correlated molecular disorder on the dynamics of excitons in organic molecular semiconductors. *J. Phys. Chem. C* **2019**, *123*, 306–314.
- (20) Varvello, L.; Lynd, J. K.; Bennett, D. I. G. Formally exact simulations of mesoscale exciton dynamics in molecular materials. *Chem. Sci.* **2021**, *12*, 9704–9711.
- (21) Campaioli, F.; Cole, J. H. Exciton transport in amorphous polymers and the role of morphology and thermalisation. *New J. Phys.* **2021**, *23*, 113038.
- (22) Giannini, S.; Peng, W.-T.; Cupellini, L.; Padula, D.; Carof, A.; Blumberger, J. Exciton transport in molecular organic semiconductors boosted by transient quantum delocalization. *Nat. Commun.* **2022**, *13*, 2755.
- (23) Sneyd, A. J.; Fukui, T.; Palecek, D.; Prodhan, S.; Wagner, I.; Zhang, Y.; Sung, J.; Collins, S. M.; Slater, T. J. A.; Andaji-Garmaroudi, Z.; MacFarlane, L. R.; Garcia-Hernandez, J. D.; Wang, L.; Whittell, G. R.; Hodgkiss, J. M.; Chen, K.; Beljonne, D.; Manners, I.; Friend, R. H.; Rao, A. Efficient energy transport in an organic semiconductor mediated by transient exciton delocalization. *Sci. Adv.* **2021**, *7*, No. eab4232.
- (24) Prodhan, S.; Giannini, S.; Wang, L.; Beljonne, D. Long-range interactions boost singlet exciton diffusion in nanofibers of π -extended polymer chains. *J. Phys. Chem. Lett.* **2021**, *12*, 8188–8193.
- (25) Kranz, J. J.; Elstner, M. Simulation of singlet exciton diffusion in bulk organic materials. *J. Chem. Theory Comput.* **2016**, *12*, 4209–4221.
- (26) Sneyd, A. J.; Beljonne, D.; Rao, A. A new frontier in exciton transport: Transient delocalization. *J. Phys. Chem. Lett.* **2022**, *13*, 6820–6830.
- (27) Balzer, D.; Smolders, T. J. A. M.; Blyth, D.; Hood, S. N.; Kassal, I. Delocalised kinetic Monte Carlo for simulating delocalisation-enhanced charge and exciton transport in disordered materials. *Chem. Sci.* **2021**, *12*, 2276–2285.
- (28) Balzer, D.; Kassal, I. Even a little delocalization produces large kinetic enhancements of charge-separation efficiency in organic photovoltaics. *Sci. Adv.* **2022**, *8*, No. eabl9692.
- (29) Bässler, H. Charge transport in disordered organic photoconductors a Monte Carlo simulation study. *Phys. Status Solidi B* **1993**, *175*, 15–56.
- (30) Fröhlich, H. Electrons in lattice fields. *Adv. Phys.* **1954**, *3*, 325–361.

- (31) Holstein, T. Studies of polaron motion: Part I. The molecular-crystal model. *Ann. Phys.* **1959**, *8*, 325–342.
- (32) Grover, M.; Silbey, R. Exciton migration in molecular crystals. *J. Chem. Phys.* **1971**, *54*, 4843–4851.
- (33) Pollock, F. A.; McCutcheon, D. P.; Lovett, B. W.; Gauger, E. M.; Nazir, A. A multi-site variational master equation approach to dissipative energy transfer. *New J. Phys.* **2013**, *15*, 075018.
- (34) Jang, S. Theory of multichromophoric coherent resonance energy transfer: A polaronic quantum master equation approach. *J. Chem. Phys.* **2011**, *135*, 034105.
- (35) Jang, S.; Cao, J.; Silbey, R. J. On the temperature dependence of molecular line shapes due to linearly coupled phonon bands. *J. Phys. Chem. B* **2002**, *106*, 8313–8317.
- (36) Wilner, E. Y.; Wang, H.; Thoss, M.; Rabani, E. Sub-Ohmic to super-Ohmic crossover behavior in nonequilibrium quantum systems with electron-phonon interactions. *Phys. Rev. B* **2015**, *92*, 44–48.
- (37) Lee, C. K.; Moix, J.; Cao, J. Accuracy of second order perturbation theory in the polaron and variational polaron frames. *J. Chem. Phys.* **2012**, *136*, 204120.
- (38) Rice, B.; Guillet, A. A. Y.; Frost, J. M.; Nelson, J. Polaron states in fullerene adducts modeled by coarse-grained molecular dynamics and tight binding. *J. Phys. Chem. Lett.* **2018**, *9*, 6616–6623.
- (39) Jang, S.; Cheng, Y.-C.; Reichman, D. R.; Eaves, J. D. Theory of coherent resonance energy transfer. *J. Chem. Phys.* **2008**, *129*, 101104.
- (40) Nazir, A. Correlation-dependent coherent to incoherent transitions in resonant energy transfer dynamics. *Phys. Rev. Lett.* **2009**, *103*, 146404.
- (41) Jang, S. Theory of coherent resonance energy transfer for coherent initial condition. *J. Chem. Phys.* **2009**, *131*, 164101.
- (42) McCutcheon, D. P. S.; Nazir, A. Coherent and incoherent dynamics in excitonic energy transfer: Correlated fluctuations and off-resonance effects. *Phys. Rev. B* **2011**, *83*, 165101.
- (43) Kolli, A.; Nazir, A.; Olaya-Castro, A. Electronic excitation dynamics in multichromophoric systems described via a polaron-representation master equation. *J. Chem. Phys.* **2011**, *135*, 154112.
- (44) McCutcheon, D. P. S.; Nazir, A. Consistent treatment of coherent and incoherent energy transfer dynamics using a variational master equation. *J. Chem. Phys.* **2011**, *135*, 114501.
- (45) McCutcheon, D. P. S.; Dattani, N. S.; Gauger, E. M.; Lovett, B. W.; Nazir, A. A general approach to quantum dynamics using a variational master equation: Application to phonon-damped Rabi rotations in quantum dots. *Phys. Rev. B* **2011**, *84*, 081305.
- (46) Lee, C. K.; Moix, J.; Cao, J. Coherent quantum transport in disordered systems: A unified polaron treatment of hopping and band-like transport. *J. Chem. Phys.* **2015**, *142*, 164103.
- (47) Xu, D.; Cao, J. Non-canonical distribution and non-equilibrium transport beyond weak system-bath coupling regime: A polaron transformation approach. *Front. Phys.* **2016**, *11*, 110308.
- (48) Lorenz, M. O. Methods of measuring the concentration of wealth. *J. Am. Stat. Assoc.* **1905**, *9*, 209–219.
- (49) Gini, C. *Variabilità e Mutabilità: Contributo allo Studio delle Distribuzioni e delle Relazioni Statistiche*; P. Cuppini: Bologna, Italy, 1912.
- (50) Giannini, S.; Carof, A.; Ellis, M.; Yang, H.; Ziogos, O. G.; Ghosh, S.; Blumberger, J. Quantum localization and delocalization of charge carriers in organic semiconducting crystals. *Nat. Commun.* **2019**, *10*, 3843.
- (51) Chang, H.-T.; Zhang, P.-P.; Cheng, Y.-C. Criteria for the accuracy of small polaron quantum master equation in simulating excitation energy transfer dynamics. *J. Chem. Phys.* **2013**, *139*, 224112.
- (52) Silbey, R.; Harris, R. A. Variational calculation of the dynamics of a two level system interacting with a bath. *J. Chem. Phys.* **1984**, *80*, 2615.
- (53) Zimanyi, E. N.; Silbey, R. J. Theoretical description of quantum effects in multi-chromophoric aggregates. *Philos. Trans. Royal Soc. A* **2012**, *370*, 3620–3637.
- (54) Jang, S. J. Partially polaron-transformed quantum master equation for exciton and charge transport dynamics. *J. Chem. Phys.* **2022**, *157*, 104107.
- (55) Jiang, X.; Brumer, P. Creation and dynamics of molecular states prepared with coherent vs partially coherent pulsed light. *J. Chem. Phys.* **1991**, *94*, 5833–5843.
- (56) Mančal, T.; Valkunas, L. Exciton dynamics in photosynthetic complexes: Excitation by coherent and incoherent light. *New J. Phys.* **2010**, *12*, 065044.
- (57) Brumer, P.; Shapiro, M. Molecular response in one-photon absorption via natural thermal light vs. pulsed laser excitation. *Proc. Natl. Acad. Sci. U. S. A.* **2012**, *109*, 19575–19578.
- (58) Kassal, I.; Yuen-Zhou, J.; Rahimi-Keshari, S. Does coherence enhance transport in photosynthesis? *J. Phys. Chem. Lett.* **2013**, *4*, 362–367.
- (59) Brumer, P. Shedding (Incoherent) light on quantum effects in light-induced biological processes. *J. Phys. Chem. Lett.* **2018**, *9*, 2946–2955.
- (60) Tomasi, S.; Baghbanzadeh, S.; Rahimi-Keshari, S.; Kassal, I. Coherent and controllable enhancement of light-harvesting efficiency. *Phys. Rev. A* **2019**, *100*, 043411.
- (61) Tomasi, S.; Kassal, I. Classification of coherent enhancements of light-harvesting processes. *J. Phys. Chem. Lett.* **2020**, *11*, 2348–2355.
- (62) Tomasi, S.; Rouse, D. M.; Gauger, E. M.; Lovett, B. W.; Kassal, I. Environmentally improved coherent light harvesting. *J. Phys. Chem. Lett.* **2021**, *12*, 6143–6151.
- (63) Willson, J. T.; Liu, W.; Balzer, D.; Kassal, I. Jumping kinetic Monte Carlo: Fast and accurate simulations of partially delocalised charge transport in organic semiconductors. *arXiv.org, e-Print Arch., Phys.* **2022**, arXiv:2211.16165.

Recommended by ACS

A Mean-Field Treatment of Vacuum Fluctuations in Strong Light-Matter Coupling

Ming-Hsiu Hsieh, Roel Tempelaar, et al.

JANUARY 31, 2023

JOURNAL OF PHYSICAL CHEMISTRY LETTERS

READ 

Factorized Electron–Nuclear Dynamics with an Effective Complex Potential

Sophya Garashchuk, Vitaly Rassolov, et al.

FEBRUARY 16, 2023

JOURNAL OF CHEMICAL THEORY AND COMPUTATION

READ 

Tensor-Train Thermo-Field Memory Kernels for Generalized Quantum Master Equations

Ningyi Lyu, Victor S. Batista, et al.

JANUARY 31, 2023

JOURNAL OF CHEMICAL THEORY AND COMPUTATION

READ 

MLRNet: Combining the Physics-Motivated Potential Models with Neural Networks for Intermolecular Potential Energy Surface Construction

You Li, Hui Li, et al.

FEBRUARY 24, 2023

JOURNAL OF CHEMICAL THEORY AND COMPUTATION

READ 

Get More Suggestions >